Measurement of step and kink energies and of the step-edge stiffness from island studies on Pt(111)

Julian Ikonomov,* Kirilka Starbova,[†] and Harald Ibach Institut für Bio- und Nanosysteme, IBN 3, Forschungszentrum Jülich, D-52425 Jülich, Germany

Margret Giesen‡

Institut für Bio- und Nanosysteme, IBN 4, Forschungszentrum Jülich, D-52425 Jülich, Germany (Received 26 February 2007; published 12 June 2007)

By using temperature-variable scanning tunneling microscopy, we studied two-dimensional vacancy islands on Pt(111) between 593 and 713 K. Due to the difference in the step free energies of A and B steps, the equilibrium shape of the vacancy islands has a threefold symmetry. From the analysis of the equilibrium shape of the vacancy islands, we calculate the angular dependence of the step free energy on Pt(111). The absolute values for the step free energies per atom of A and B steps are determined from the equilibrium shape fluctuations to be β_A =348±16 meV/atom and β_B =300±14 meV/atom, respectively. Furthermore, we derive the temperature dependence of the step-edge stiffness $\tilde{\beta}$ with $\tilde{\beta}_A$ between 510 and 453 meV/atom and $\tilde{\beta}_B$ between 1974 and 1104 meV/atom in the temperature range considered. From the stiffness, we obtain the kink formation energies for A and B steps, ε_A =143±9 meV and ε_B =206±9 meV, respectively.

DOI: 10.1103/PhysRevB.75.245411 PACS number(s): 68.08.-p, 68.37.Ef

I. INTRODUCTION

One of the most important energy parameters that determines equilibrium as well as nonequilibrium properties of crystals and of crystal surfaces is the step line tension defined as the work per unit length (or per step atom) needed to create a step. For uncharged surfaces in vacuum, the step line tension is equal to the (Helmholtz) free energy of a step. It can be understood as the one-dimensional analog to the surface tension, which is the free energy per unit area on uncharged surfaces in vacuum. The step free energy (and its dependence on the step-step distance) determines the equilibrium shape of crystals.^{2,3} It is also the driving force for coarsening phenomena on surfaces such as two-dimensional Ostwald ripening and therefore a key parameter in epitaxial growth. Nevertheless, it was only recently that methods were established to determine the step line tension experimentally, e.g., from the temperature dependence of the equilibrium shape of islands on surfaces⁴ and from the equilibrium fluctuations of the island perimeter.⁵⁻⁷ The free energies of steps on Ag(111), Cu(111), Cu(100), and TiN(111) and TiN(100) have been measured employing these methods.⁶⁻¹¹ In particular, Kodambaka et al. presented for the first time data on the orientation dependence of step energies and step stiffnesses from island studies on TiN(111) (Refs. 12 and 13) and (100) (Refs. 9 and 11) surfaces. Recent studies also include steps on charged metal surfaces in contact with an electrolyte^{14,15} (where the step line tension differs from the free energy^{16,17}).

Here, we present the experimental study on the step line tension of the Pt(111) surface, a surface that was otherwise extensively studied in the past and has served as a model for epitaxial growth on metals. Using scanning tunneling microscopy (STM), we have measured the equilibrium shape of (vacancy) islands in the temperature range between 593 and 713 K. From an inverse Wulff construction on the equilibrium shape, the angular dependence of the step line tension is

obtained. We have furthermore analyzed the equilibrium fluctuations of islands in the same temperature range, which renders the mean absolute value of the step line tension. Combining the two results, we obtain specifically absolute values for the step free energies per atom of A and B steps [steps displaying (100) and (111) facets, respectively]. From the angle dependence of the step free energy, we furthermore derive the step-edge stiffness. Within the framework of a low-temperature approximation, kink energies for A and B steps are calculated. While our results on the step line tension and kink energies are by and large in keeping with previous theoretical studies, the values for the stiffness of A and B steps differ significantly from those reported recently for Pt(111) at high temperatures. 19

The paper is organized as follows. Section II describes the experimental procedures. Section III provides a brief summary of the relevant theoretical equations needed for the analysis. Experimental results are presented in Sec. IV. Section V discusses the results in the context of previous theoretical and experimental studies.

II. EXPERIMENT

The experiments were performed in a standard ultrahigh-vacuum chamber equipped with a temperature-variable microscope 20,21 with high thermal drift stability. The Pt(111) samples were cut from a (111) single-crystal rod by spark erosion. They were polished and oriented by diffractometry to the desired orientation within 0.1°. The surface was cleaned by repeated cycles of ion sputtering $(5.5 \times 10^{-5}$ mbar Ne, 3 kV, 10 μ A sputter current) and subsequent annealing to 1200 K.²² After 15–20 cycles, the Auger spectrum showed no residual carbon contamination on the Pt samples. Since the detection limit of the Auger spectrometer is about 1%, some carbon contamination was, however, still visible in the STM images after 15–20 preparation cycles.

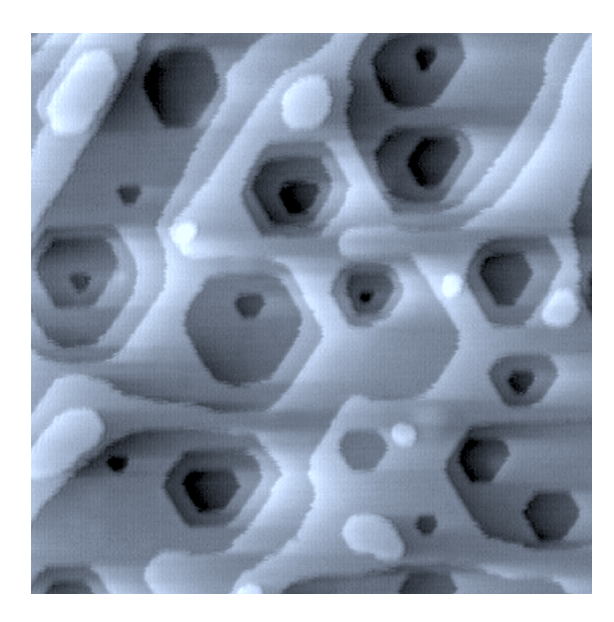


FIG. 1. STM image of the Pt(111) surface with vacancy islands at T=593 K. The scan width is 97.6 nm.

Therefore, the surface cleaning was extended to about 30 cycles after which no surface contamination was detectable in STM. The vacancy islands were produced by Ne sputtering (1 kV, 5 μ A) at the temperature where the measurements eventually were performed. As an example, Fig. 1 shows a STM image of vacancy islands on Pt(111) at 593 K. For the analysis, we used exclusively islands in equilibrium as indicated by the presence of island perimeter fluctuations and the absence of pinning points on the perimeter. Furthermore, we analyzed exclusively islands, which were free to move and were not restricted by the presence of step and island edges in close vicinity.

The tunneling tip was made from polycrystalline tungsten wire by electrochemical etching. In the experiments, we used a tunneling current of 2 nA and a tunneling bias of 0.6 V which are appropriate values to prevent an influence of the tunneling tip on the surface atomic motion on Pt(111).²³ The STM images were analyzed using the computer codes described in detail in Refs. 4 and 24.

The island perimeter on (111) surfaces contains two types of steps with different atomic configurations at the step edges (Fig. 2): A and B steps forms (100) and (111) microfacets with the underlying terrace, respectively. In general, the two steps have different energies, although the difference may be small. In the case of Cu(111) and Ag (111) for instance, Aand B-step energies differ by less than 1%. ^{4,6,7} Consequently, the equilibrium shapes of islands on these surfaces have nearly sixfold symmetry. For Pt(111), Michely and Comsa determined the energy ratio between A and B steps to be 1.15 for temperatures between 700 and 925 K.²² The island equilibrium shape on Pt(111) therefore resembles a truncated triangle and the symmetry of the islands is visibly threefold. This is demonstrated in the STM image of a vacancy island on Pt(111), as shown in Fig. 3(a). The short frizzes visible at the inner vacancy island edge in Fig. 3(a) are due to the rapid motion of kinks at the island perimeter^{25,26} and represent another manifestation of the perimeter equilibrium fluctuations.

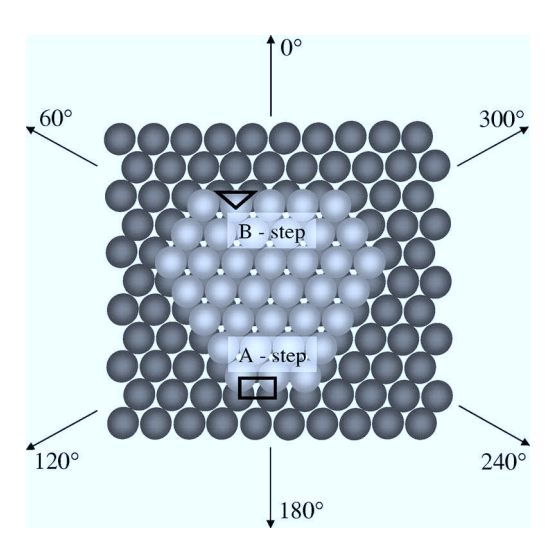


FIG. 2. Atomic ball model of an island on a fcc (111) surface. The geometry of alternating island edges is different: A and B steps form (100) and (111) microfacets, respectively, with the underlying terrace. For Pt(111), A and B steps have considerably different energies; hence, the islands display a threefold symmetry.

Islands on crystal surfaces fluctuate around their equilibrium shape at finite temperature due to attachment-detachment processes of individual atoms and diffusion processes along the island perimeter. 5-7,12,14 In order to measure the equilibrium shape of islands at a distinct temperature, one has to average over many individual island shapes. The total number of individual islands and island shapes required to determine the equilibrium shape depends on the system and on the temperature. The number typically ranges from at least 100 up to several hundreds of island shapes. As an example, Fig. 3(b) displays the perimeter of the vacancy is-

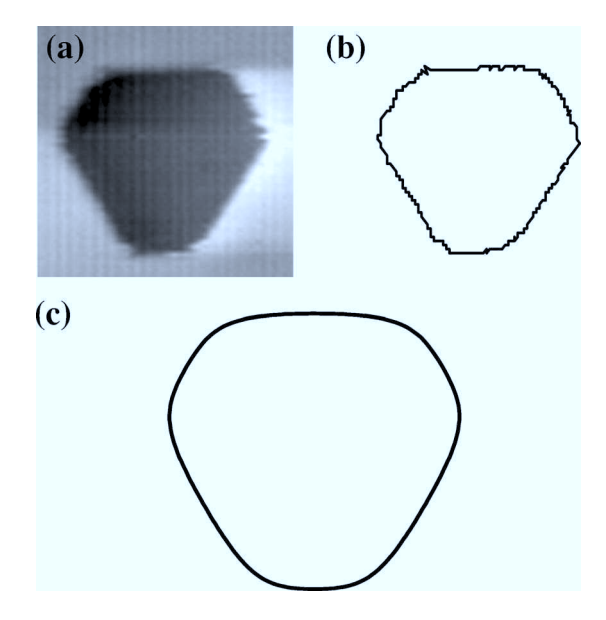


FIG. 3. (a) STM image of a vacancy island on Pt(111) at 633 K. The scan width is 15.2 nm. (b) Island perimeter of the vacancy island as shown in (a) as obtained from the used computer code. (c) Equilibrium island shape for Pt(111) at 633 K as found after averaging over more than 800 individual island shapes, as shown in (b).

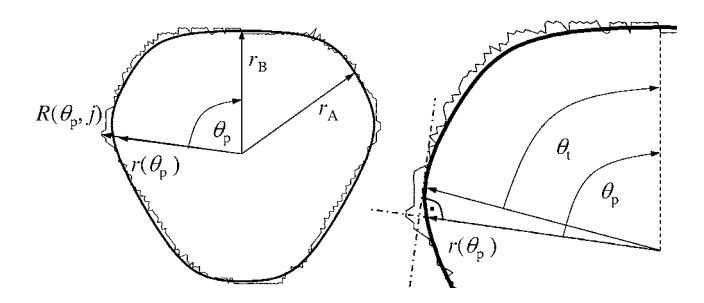


FIG. 4. Equilibrium shape (bold solid line) and an island perimeter as obtained from an individual island in a particular STM image (thin solid line). Both shapes are normalized to have the same area. The deviation of the individual shape from the equilibrium shape is used to determine the fluctuation correlation function [Eqs. (4) and (5)] and from that the step line tension. See text for further discussion.

land in Fig. 3(a) as detected by our computer code. The corresponding equilibrium shape obtained by averaging over more than 800 individual island shapes at 633 K is shown in Fig. 3(c).

The computer code determines the island perimeter in polar coordinates with the center of mass as the origin. In order to compare and average the shapes of islands of different sizes, the island areas are normalized. In total, we analyzed 4500 islands at six different temperatures between 593 and 713 K.

III. THEORY OF ISLAND SHAPE ANALYSIS

The island shape fluctuations are analyzed by comparing the island perimeter in a distinct STM image with the equilibrium shape at the same temperature. The procedure is illustrated in Fig. 4. Here, $R(\theta_p,j)$ and $r(\theta_p)$ are vectors that define the perimeter of an island in a particular STM frame j and the equilibrium island shape, respectively, where θ_p is the polar angle. The relative difference of $R(\theta_p,j)$ and $r(\theta_p)$ in polar coordinates is denoted as

$$g(\theta_p, j) = \frac{R(\theta_p, j) - r(\theta_p)}{r(\theta_p)}.$$
 (1)

A measure of the island perimeter fluctuations is

$$G(\overline{r},j) = \frac{\overline{r}^2}{2\pi} \int_0^{2\pi} g^2(\theta_p,j) d\theta_p, \tag{2}$$

where \bar{r} is the mean radius of an equilibrium island written in terms of the angle-dependent island radius $r(\theta_n)$ as

$$\bar{r} = \frac{1}{2\pi} \int_0^{2\pi} r(\theta_p) d\theta_p. \tag{3}$$

For the isotropic case, the ensemble averaged fluctuation function can be written as⁶

$$\langle G(\overline{r})\rangle_{j} = \frac{3k_{B}\overline{r}T}{4\pi\overline{\beta}},\tag{4}$$

where k_B is the Boltzmann constant, T the temperature, and $\bar{\beta}$ the mean step free energy per length (in general, the line

tension¹). Hence, $\bar{\beta}$ may be obtained by measuring the averaged perimeter fluctuations for different mean island sizes. Equation (4) holds for the isotropic case; however, it proves to be a good approximation for island fluctuations on Cu(111), Ag(111) where the anisotropy of the step free energy is small.^{6,7,27} In the case of Pt(111), however, the anisotropy of the step free energy is larger and Eq. (4) is to be replaced by⁷

$$\langle G(\vec{r})\rangle_j = \frac{k_B \vec{r} T}{2\pi \bar{\beta}} \sum_{|n|>1} \frac{1}{n^2 - \alpha}.$$
 (5)

Here, α is an "anisotropy" factor which is defined as

$$\alpha = \frac{1}{2\pi} \int_{0}^{2\pi} \frac{\beta(\theta_p) \sqrt{r(\theta_p) + \left[\frac{\partial r(\theta_p)}{\partial \theta_p}\right]^2}}{\bar{\beta}\bar{r}}.$$
 (6)

The anisotropy factor α is $\alpha=1$ for a circle and 1.028 for Cu(111) at 313 K. The sum in Eq. (5) yields 3/2 and 1.507, respectively. Hence, for Cu(111), the isotropic model [Eq. (4)] is a good approximation. However, for the more anisotropic islands on Pt(111), the use of Eq. (5) is preferred.

According to Ref. 7, there is a direct relation between the mean step free energy $\bar{\beta}$ and the angle-dependent, absolute step free energy $\beta(\theta)$:

$$\bar{\beta} = \frac{1}{2\pi} \int_0^{2\pi} \left[\frac{\beta(\theta_p)}{\bar{r}} \frac{r^4(\theta_p)}{\left\{ r^2(\theta_p) + \left[\frac{\partial r(\theta_p)}{\partial \theta_p} \right] \right\}^{3/2}} \right] d\theta_p. \quad (7)$$

Dividing both sides of Eq. (7) by $\beta(\theta=0)=\beta_B$, as well as multiplying the integrand by r_B^4/r_B^4 , yields

$$\frac{\bar{\beta}}{\beta_B} = \frac{1}{2\pi} \int_0^{2\pi} \left[\frac{\frac{\beta(\theta_p)}{\beta_B}}{\frac{\bar{\beta}_B}{r_B^4}} \frac{\frac{r^4(\theta_p)}{r_B^4}}{\frac{\bar{r}}{r_B^4}} \left\{ r^2(\theta_p) + \left[\frac{\partial r(\theta_p)}{\partial \theta_p} \right] \right\}^{3/2} \right] d\theta_p.$$
(8)

Now, we have in principle a tool to determine absolute values of step free energies for A and B steps: $\beta(\theta_p)/\beta_B$ can be determined using the angular anisotropy of the step free energy $\beta(\theta_t)$ as obtained from the island equilibrium shape via the inverse Wulff construction.²⁸ As a caveat, we emphasize that the angle dependence of the step free energy as obtained from the inverse Wulff construction is given with respect to the tangential angle θ_t (see Fig. 4. for the definition of θ_t) rather than to the polar angle θ_p . Therefore, from both angles θ_t and θ_p , only the tangential angle yields the meaningful physical information. There is, however, a simple relation between θ_p and θ_t (Ref. 29):

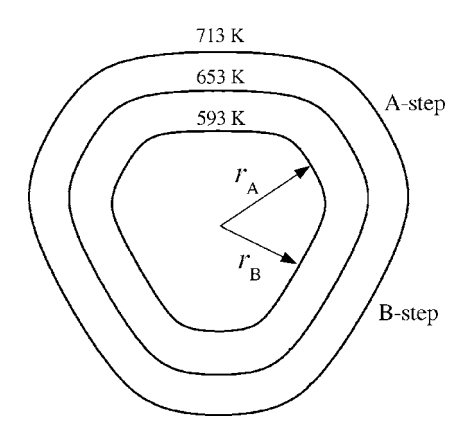


FIG. 5. Equilibrium island shapes for Pt(111) at various temperatures.

$$\theta_p = \theta_t + \arctan\left(\frac{\frac{\partial \beta(\theta_t)}{\partial \theta_t}}{\beta(\theta_t)}\right). \tag{9}$$

Since $\bar{\beta}$ is obtained from island shape fluctuations in a certain temperature regime (in our experiments between 593 and 713 K), the ratio $\beta(\theta_p)/\beta_B$ is a temperature-dependent function. Because of the smallness of the anisotropy and the temperature dependence, it suffices to evaluate Eq. (8) with data for $\beta(\theta_p)/\beta_B$ at a single intermediate temperature (T=653 K in our case). We emphasize that the complete angular dependence of the step free energy can only be obtained if the two-dimensional equilibrium shape of islands has no facets or sign changes in the curvature. So far, facets have never been observed on islands. Thus, steps seem to behave as one-dimensional objects, which are thermodynamically rough at any finite temperature. Furthermore, islands of three- and fourfold symmetries studied so far all retain the same sign of the curvature along the perimeter.

From the angular anisotropy of the step free energy $\beta(\theta_t)$, one can deduce the step-edge stiffness $\tilde{\beta}(\theta_t)$ which is related to $\beta(\theta_t)$ via^{23,30}

$$\widetilde{\beta}(\theta_t) = \beta(\theta_t) + \frac{\partial^2 \beta(\theta_t)}{\partial \theta_t^2}.$$
 (10)

Alternatively, one can determine the stiffness directly from the equilibrium shape by using a relation which combines Wulff's theorem with the Herring-Mullins equation (see, e.g., Refs. 1 and 27)

$$\widetilde{\beta}(\theta_t)\kappa(\theta_t) = \beta_A/r_A = \beta_B/r_B,\tag{11}$$

where $\kappa(\theta_t)$ denotes the curvature of the crystal equilibrium shape. The step stiffness is generally related to the diffusivity b^2 via^{23,30}

$$b^2 = \frac{k_B T}{\tilde{\beta}} a_{\parallel},\tag{12}$$

with a_{\parallel} the nearest-neighbor atomic distance along the $\langle 110 \rangle$ -crystal direction [for Pt(111), a_{\parallel} =2.77 Å]. For steps oriented along the direction of dense packing (A and B steps), the

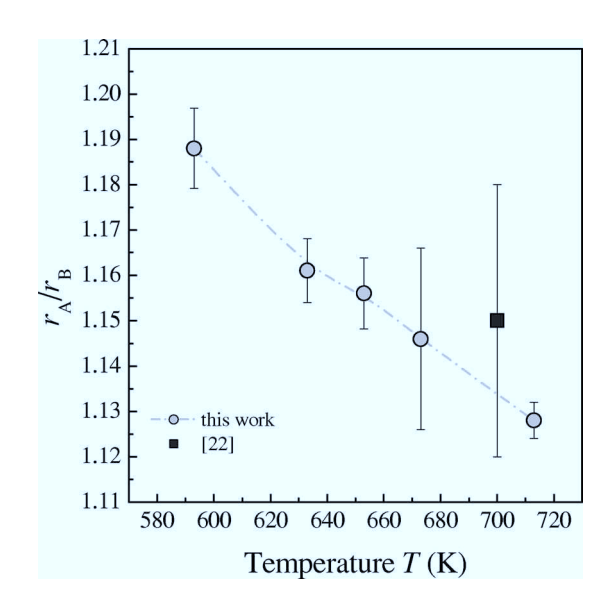


FIG. 6. Temperature dependence of the ratio r_A/r_B (circles) of the radii in the equilibrium shape at angles θ_p =60° and 0°, corresponding to the ratio β_A/β_B of the step free energies of A and B steps. The square refers to a data point as reported in Ref. 22.

diffusivity can be expressed in terms of the kink energy ε (Ref. 26) if the temperature is not too high,

$$b_{A,B}^2 \approx 2a_\perp^2 \exp(-\varepsilon_{A,B}/k_BT), \quad \exp(-\varepsilon_{A,B}/k_BT) \ll 1.$$
 (13)

Here, a_{\perp} is the distance between densely packed atomic rows $[a_{\perp} = (\sqrt{3}/2)a_{\parallel} = 2.40 \text{ Å} \text{ for Pt(111)}]$. Combining Eqs. (11)–(13) yields²⁷

$$\varepsilon_{A,B} \cong -k_B T \ln[(2k_B T)/(3a_{\parallel} \widetilde{\beta}_{A,B})]$$

= $-k_B T \ln[(2r_{A,B} \kappa_{A,B} k_B T)/(3a_{\parallel} \beta_{A,B})].$ (14)

Here, $\kappa_{A,B}$ denotes the curvature of the crystal equilibrium shapes in the orientation that corresponds to A and B steps. These curvatures are reliably obtained only if the temperature is not too small. In our experiments, this was the case for the entire temperature range between 593 and 713 K.

IV. EXPERIMENTAL RESULTS

Figure 5 shows measured equilibrium shapes of vacancy islands on Pt(111) for three different temperatures. In agreement with the studies of Michely and Comsa, 22 the "length" of A step segments is smaller than the "length" of B step segments, indicating that A steps have the higher step formation energy compared to B steps. Figure 6 shows the ratio r_A/r_B vs temperature as light gray circles. The ratio r_A/r_B decreases with increasing temperature with $r_A/r_B \sim 1.19$ at 593 K and 1.13 at 713 K in agreement with the data by Michely and Comsa 22 plotted as dark gray square in Fig. 6. The decrease of r_A/r_B with T results in a rounding of the island equilibrium shape at higher temperatures (Fig. 5).

Applying the inverse Wulff construction^{7,28} to the equilibrium shapes of the Pt(111) vacancy islands yields the Wulff plot $\beta(\theta_t)/\beta_B$ for Pt(111) which is shown in Fig. 7(a) for

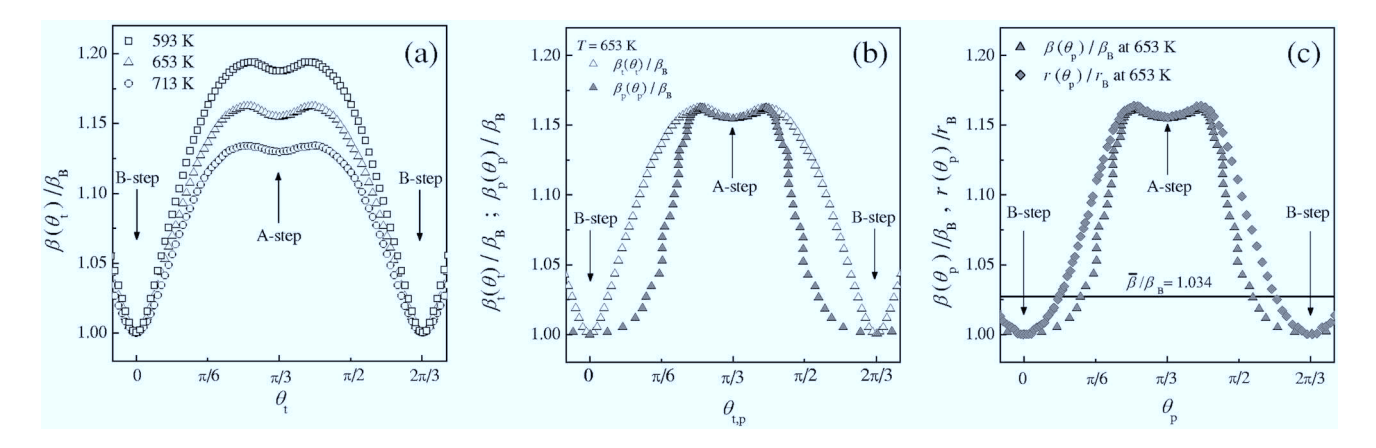


FIG. 7. (a) $\beta(\theta_t)$ for Pt(111) for three different temperatures T=593 K (squares), T=653 K (triangles), and T=713 K (circles). The values are normalized to the free energy β_B of the B step. (b) Comparison of $\beta(\theta_t)$ (open triangles) and $\beta(\theta_p)$ (filled triangles) for Pt(111) at 653 K. (c) Plot of $\beta(\theta_p)/\beta_B$ (filled triangles) and $r(\theta_p)/r_B$ (filled diamonds) at an intermediate temperature of 653 K to determine the absolute step free energies β_A and β_B . See text for further discussion.

three different temperatures. Due to the threefold symmetry of the islands, the Wulff plot is periodic in $2/3\pi$ and Fig. 7(a) displays merely the range between 0 and $2/3\pi$. The values at 0 and $1/3\pi$ correspond to the step free energies of B and A steps, respectively. The data points are normalized with respect to the free energy of the B step. Because of the mirror symmetry around the orientation of A and B steps, the ratio β_A/β_B equals the ratio of the radii r_A/r_B (Fig. 6). Hence, one can directly obtain the relative step free energies from the equilibrium shapes. For T=593 K, we find β_A/β_B =1.19 and for T=713 K, $\beta_A/\beta_B=1.13$. For comparison, Fig. 7(b) displays $\beta(\theta_t)/\beta_B$ (open triangles) as well as $\beta(\theta_p)/\beta_B$ (filled triangles). For the regions around β_A and β_B , both curves coincide. For angles in between $\beta(\theta_t)/\beta_B$ and $\beta(\theta_p)/\beta_B$ deviate significantly. This is not due to an experimental error. Rather the differences in the definition of the tangential and the polar angle as shown in Fig. 4 give rise to the differences in $\beta(\theta_t)/\beta_B$ and $\beta(\theta_p)/\beta_B$. Although the polar angle is easily accessible from experimental data of island shapes, the tangential angle yields the physically meaningful information. Figure 7(c) shows $\beta(\theta_p)/\beta_B$ (gray triangles) and $r(\theta_p)/r_B$ (gray diamonds) for Pt(111) at T=653 K. By calculating the integrals in Eqs. (6) and (8), we derive the anisotropy factor α for Pt(111) to be 1.060 and the sum in Eq. (5) yields 1.516. Furthermore, we obtain $\bar{\beta}/\beta_B = 1.034$.

In order to determine the absolute values of the step free energies, the island shape fluctuations are analyzed according to Eq. (5) with the help of Eqs. (6) and (8). Figure 8 shows $\langle G(\vec{r})\rangle_j$ plotted vs the product of the mean island radius \vec{r} and temperature T between 593 and 713 K. According to Eqs. (4) and (5), the slope of the linear fit is inversely proportional to the mean step free energy per atom unit. From Fig. 8, one finds a slope $(1.856\pm0.085)\times10^{-5}$ nm/K, which corresponds to

$$a_{\parallel}\bar{\beta} = 310 \pm 14 \text{ meV},$$
 (15)

with α =1.060. Using $\bar{\beta}/\beta_B$ =1.034 and β_A/β_B =1.16±0.01 as the aspect ratio at T=653 K, we then obtain for the abso-

lute values of the step free energies of A and B steps on Pt(111)

$$a_{\parallel}\beta_A = 348 \pm 16 \text{ meV}$$
 and $a_{\parallel}\beta_B = 300 \pm 14 \text{ meV}$. (16)

According to Eq. (10), one may calculate the angle-dependent stiffness $\tilde{\beta}(\theta_t)$ from the data for $\beta(\theta_t)$. Of particular interest is the stiffness of A and B steps. By numerical differentiation, we obtain from Fig. 7 for T=653 K, $a_{\parallel}\tilde{\beta}_A \sim 0.5$ eV and $a_{\parallel}\tilde{\beta}_B \sim 1.4$ eV.

By using Eq. (11), one can also determine the stiffness from the product of curvature and radius and the step energy. Table I shows the minimum curvatures on the equilibrium shapes for the *A*- and *B*-oriented steps for three temperatures.

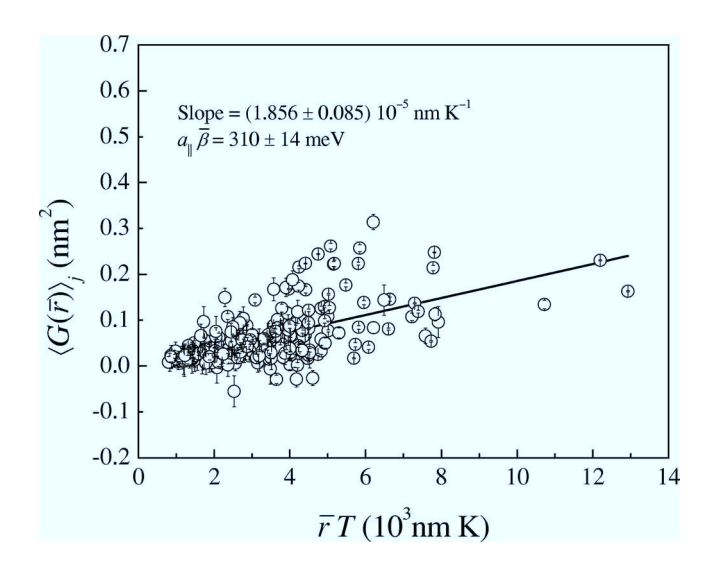


FIG. 8. The ensemble averaged fluctuation function $\langle G(\bar{r}) \rangle_j$ vs the product of the mean island radius \bar{r} and temperature T [Eq. (5) with α =1.060 and $\Sigma_{|n|>1}1/(n^2-\alpha)$ =1.516]. According to Eq. (5), one obtains the mean step free energy $\bar{\beta}$ from the slope of a linear fit to the data.

TABLE I. Experimental data on the products of curvatures and radial distances from the center for three equilibrium shapes together with the calculated stiffness $a_{\parallel}\widetilde{\beta}_{A}$ and $a_{\parallel}\widetilde{\beta}_{B}$ and the corresponding kink energies ε_{A} and ε_{B} . Curvatures were calculated by fitting the experimental data in a range of $\pm 5^{\circ}$ and $\pm 10^{\circ}$ for A and B steps, respectively. The errors in the curvature are the statistical errors of the fitting procedure. The errors in $a_{\parallel}\widetilde{\beta}$ and ε include the errors of $a_{\parallel}\beta$. Note that $a_{\parallel}=0.277$ nm for Pt(111).

Temperature (K)	$r_A \kappa_A$	$a_{\parallel}\widetilde{\beta}_{A} \; (\text{meV})$	$\varepsilon_A \; (\text{meV})$	$r_B \kappa_B$	$a_{\parallel} \tilde{\beta}_{B} \; (\text{meV})$	$\varepsilon_B \; (\text{meV})$
593	0.708 ± 0.010	492 ± 32	136±3	0.152 ± 0.004	1974±138	207 ± 4
653	0.722 ± 0.013	482 ± 32	144 ± 3	0.204 ± 0.005	1471 ± 102	206 ± 4
713	0.769 ± 0.007	453 ± 30	148 ± 3	0.288 ± 0.012	1042 ± 70	199±4

From this, we obtain the temperature-dependent step stiffness according to Eq. (11). In total, we could analyze the curvature and stiffness for five different temperatures. The result is displayed in Fig. 9 as open squares (A steps) and circles (B steps). $\tilde{\beta}_A$ depends merely weakly on temperature between 593 and 713 K. In contrast, $\tilde{\beta}_B$ shows a strong temperature dependence. According to Eq. (14), we derive from the island edge curvature and the step-edge stiffness also the kink energies of A and B steps (Table I shows the results for three different temperatures). Using all data as shown in Fig. 9, we obtain for the kink energies

$$\varepsilon_A = 143 \pm 9 \text{ meV}$$
 and $\varepsilon_B = 206 \pm 9 \text{ meV}$. (17)

V. DISCUSSION

Our values for the step free energies of A and B steps were obtained using the perimeter fluctuation function for

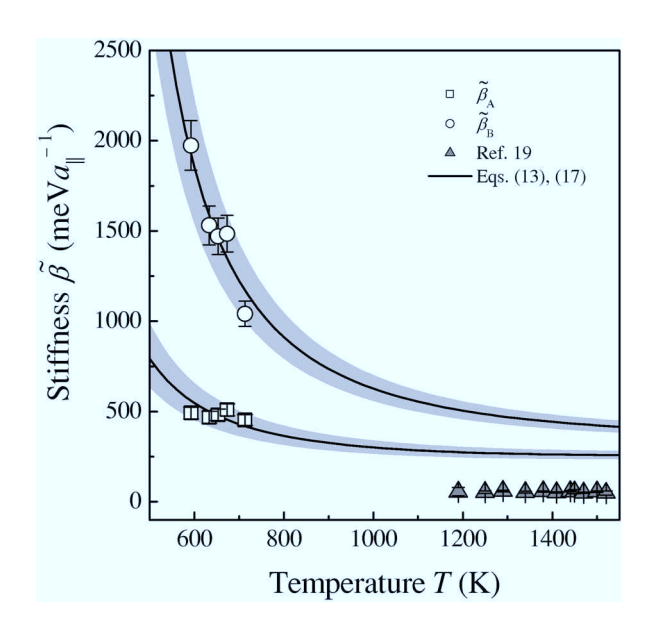


FIG. 9. Step-edge stiffness as obtained from the island edge curvature according to Eq. (11) for A (squares) and B steps (circles) on Pt(111). The solid lines show the expected temperature dependence of the stiffness using kink energies ε_A =143 meV and ε_B =206 meV in Eq. (13). The gray shaded areas around the solid lines represent the error margins ± 9 meV of the kink energies. The data plotted as gray triangles are taken from Ref. 19.

anisotropic islands [Eq. (5)]. For comparison, if one would have used the fluctuation function for the isotropic case [Eq. (4), α =1], one would have found $a_{\parallel}\bar{\beta}$ =307 meV, $a_{\parallel}\beta_A$ =344 meV, and $a_{\parallel}\beta_B$ =297 meV, which are marginally smaller values and well within the error margins. Hence, even in the case of threefold symmetry islands on Pt(111) with an anisotropy in the step energies up to 19%, the use of Eq. (4) is still a very good approximation.

Our results may be compared with experimental data of Michely and Comsa²² as well as with theoretical results of Feibelman *et al.*³¹ and Feibelman,^{32–34} Boisvert *et al.*,³⁵ and Nelson *et al.*³⁶ Table II summarizes the experimental and theoretical data for $\bar{\beta}$, β_A , β_B , ε_A , ε_B and the stiffnesses $\tilde{\beta}_A$, $\tilde{\beta}_B$. Michely and Comsa²² studied the shape of vacancy islands on Pt(111) at room temperature after annealing to temperature above 700 K. They determined the length ratio of A and B steps to be 0.66 ± 0.05 , from which a ratio r_A/r_B of 1.15 ± 0.03 was deduced. Depending on the unspecified cooling rate in their experiments, the islands in their experiment may correspond to the equilibrium shape somewhere between 600 and 700 K, which brings the result in agreement with Fig. 6.

The experimental step free energies β_A and β_B of A and B steps obtained at temperatures around 653 K are slightly smaller than the energies (i.e., the free energy at T=0 K) calculated in the local density approximation (LDA). Feibelman, e.g., finds $a_{\parallel}\beta_A=400 \text{ meV}$; $a_{\parallel}\beta_B=350 \text{ meV}$. Where $a_{\parallel}\beta_A=400 \text{ meV}$ Even larger values were obtained by Boisvert et al. 35 $(a_{\parallel}\beta_A)$ =430 meV; $a_{\parallel}\beta_{B}$ =380 meV). Using embedded atom method (EAM) calculations, Nelson et al. 36 determined step energies of $a_{\parallel}\beta_A=344$ meV and $a_{\parallel}\beta_B=341$ meV. In order to discuss these theoretical results in the light of our experimental data, one needs to extrapolate the experimental results to T=0 K. The by far largest contribution to the temperature dependence of the step free energy is owed to the entropy of phonons. In general, it can be argued that step atoms have a lower coordination and their vibration spectrum has therefore more weight in the low-frequency regime, which renders a larger vibrational entropy of step-edge atoms. At temperatures larger than the Debye temperature, the step free energy is well described by the form¹

$$f(T) = f(0) - ck_B T, (18)$$

TABLE II. Experimental and theoretical data for the step free energy, the kink energy, and the step stiffness on Pt(111) as obtained in this work and as reported in other authors' publications. All energies are in meV. Note that a_0 =0.277 nm for Pt(111).

	$a_{\parallel}ar{oldsymbol{eta}}$	$a_{\parallel}oldsymbol{eta}_{A}$	$a_{\parallel}oldsymbol{eta}_B$	$a_{\parallel}oldsymbol{eta}_{A}/a_{\parallel}oldsymbol{eta}_{B}$	$oldsymbol{arepsilon}_A$	ε_B	$a_{\parallel}\widetilde{oldsymbol{eta}}_{A}$	$a_{\parallel}\widetilde{oldsymbol{eta}}_{B}$
Experiment (this work): (593 < T < 713 K)	310±14	348±16	300 ± 14	1.19 to 1.13 (±0.01)	143±9	206±9	510 to 453	1974 to 1104
Expt. ^a (T \cong 600-700 K)				1.15 ± 0.03				
Expt. ^b (1190 < T < 1520 K)							~60	~60
Expt. ^c (<i>T</i> =540 K)					167	167		
LDA $(T=0 \text{ K})^d$		400	350	1.14	180	250		
LDA $(T=0 \text{ K})^e$		430	380	1.14				
EAM^{f}		344	341	1.01				

^aReference 22.

with a constant c that is of the order of 1 but depends on the type of surface and the type of step. Durukanoglu and Rahman have calculated the temperature dependence of the step free energy for A and B steps on Cu(111) surfaces.³⁷ If one extrapolates their results to 653 K, one finds downshifts in the free energy from T=0 to 653 K by 48 and 32 meV for A and B steps, respectively. Since the general structures of the phonon spectra of Pt and Cu are similar, and since the step free energy depends only on the ratio of step atom frequencies to bulk atom frequencies, it may be legitimate to transfer the temperature dependence from copper to platinum. The experimental step energies would then extrapolate to T=0 K as

$$a_{\parallel}\beta_A(T=0 \text{ K}) = 396 \pm 16 \text{ meV},$$

$$a_{\parallel}\beta_{B}(T=0 \text{ K}) = 332 \pm 15 \text{ meV},$$
 (19)

in excellent agreement with LDA calculations, in particular, those of Feibelman³⁴ (Table II).

Recently, Ondrejcek *et al.* measured the step-edge stiffness on Pt(111) using low-energy-electron msicroscopy in the temperature regime 1190 K \leq $T \leq$ 1520 K (gray triangles in Fig. 9).¹⁹ The authors report an average value for the stiffness of $\tilde{\beta}$ =210 meV/nm corresponding to $a_{\parallel}\tilde{\beta}$ =60 meV. In order to compare our results to the data of Ondrejcek *et al.*, we employ Eq. (13) with the experimental kink energies [Eq. (17)] inserted to extrapolate $\tilde{\beta}_A$ and $\tilde{\beta}_B$ into the temperature regime 1190 K \leq $T \leq$ 1520 K (solid lines in Fig. 9). The extrapolated curves run high compared to the result of Ondrejcek *et al.* and further indicate a considerable remaining anisotropy in $\tilde{\beta}$, which is at variance with Ondrejcek *et al.*¹⁹ We note, however, that Eq. (13) is a valid expression for the diffusivity only in the low-temperature limit [exp($-\varepsilon_k/k_BT$) \leq 1]. The deviation between

the extrapolated curves for $\tilde{\beta}_A(T)$ and $\tilde{\beta}_B(T)$ and the experimental result of Ondrejcek *et al.* may merely indicate that the stiffness drops faster with temperature than predicted by Eq. (13). Possible reasons for a faster drop include the excitation of kinks of multiple length, an increasing phonon entropy in the step free energy because of anharmonic effects, and a temperature dependence of the kink energy itself.

We cannot completely dismiss though the alternative that our data and the data of Ondrejcek *et al.* refer to a different state of the surface. A phase transition is known to occur on the clean surface at 1330 K where Pt(111) reconstructs in a fashion similar to Au(111).³⁸ The transition temperature shifts downwards under the influence of an ambient Pt-vapor pressure and in the presence of impurities.^{39,40}

Finally, we discuss the kink energies. The present values are comparable to the result of a STM study on step fluctuations around T=540 K several years ago⁴¹ where $\varepsilon_A \approx \varepsilon_B$ \approx 167 meV was found. Contrary to that earlier study, ε_R is found to be distinctly larger than ε_A . The experimental kink energies are smaller than those calculated by Feibelman³⁴ for $T=0 \text{ K } (\varepsilon_A=180 \text{ meV} \text{ and } \varepsilon_B=250 \text{ meV})$. As in the case of the step energies, the deviation may have to be attributed to the temperature dependence of the free energy. Kara and Rahman have recently reported that the free energy of kink atoms on A steps on Cu(111) surfaces has about the same temperature dependence as step atoms. 42 Taking the temperature shifts to be the same as for the step energies on Cu(111) surfaces, one would extrapolate our experimental kink energies to ε_A =195 meV and ε_B =241 meV at T=0 K, thereby nicely matching the theoretical result of Feibelman.³⁴

VI. SUMMARY

By measuring equilibrium shapes and the equilibrium perimeter fluctuations of vacancy islands on Pt(111), we have

^bReference 19.

^cReference 41.

^dReference 34.

eReference 35.

fReference 36.

derived the angular anisotropy of the step free energy and the step-edge stiffness as well as absolute values of free step and kink energies of A and B steps. Our results are in good agreement with theoretical data and with previous experiments, where existent.

ACKNOWLEDGMENTS

We acknowledge the skillful sample preparation by Udo Linke. Furthermore, J.I. and M.G. are grateful for helpful discussions with Thomas Michely. Partial support by the Fond der Chemischen Industrie is greatly appreciated.

- *Present address: Institut für Physikalische und Theoretische Chemie, Universität Bonn, Wegelerstr. 12, D-53115 Bonn, Germany
- [†]Present address: Central Laboratory of Photoprocesses, Acad. G. Bonchev Str. Bl. 109, Sofia 1113, Bulgaria.
- [‡]Corresponding author: URL: http://www.fz-juelich.de/isg/index.php?index=225. Electronic address: m.giesen@fz-juelich.de
- ¹H. Ibach, *Physics of Interfaces* (Springer, Berlin, 2006).
- ²C. Jayaprakash, C. Rottman, and W. F. Saam, Phys. Rev. B 30, 6549 (1984).
- ³H. P. Bonzel, Surf. Sci. **328**, L571 (1995).
- ⁴G. Schulze Icking-Konert, M. Giesen, and H. Ibach, Phys. Rev. Lett. 83, 3880 (1999).
- ⁵S. V. Khare and T. L. Einstein, Phys. Rev. B **54**, 11752 (1996).
- ⁶D. C. Schlößer, L. K. Verheij, G. Rosenfeld, and G. Comsa, Phys. Rev. Lett. **82**, 3843 (1999).
- ⁷C. Steimer, M. Giesen, L. Verheij, and H. Ibach, Phys. Rev. B **64**, 085416 (2001).
- ⁸ S. Kodambaka, S. V. Khare, I. Petrov, and J. E. Greene, Surf. Sci. Rep. **60**, 55 (2006).
- ⁹S. Kodambaka, S. V. Khare, V. Petrova, A. Vailionis, I. Petrov, and J. E. Greene, Surf. Sci. 513, 468 (2002).
- ¹⁰ S. Kodambaka, V. Petrova, S. V. Khare, D. D. Johnson, I. Petrov, and J. E. Greene, Phys. Rev. Lett. **88**, 146101 (2002).
- ¹¹ S. Kodambaka, S. V. Khare, V. Petrova, A. Vailionis, I. Petrov, and J. E. Greene, Surf. Sci. **523**, 316 (2003).
- ¹²S. Kodambaka, V. Petrova, S. V. Khare, D. D. Johnson, I. Petrov, and J. E. Greene, Phys. Rev. Lett. 88, 146101 (2002).
- ¹³ S. Kodambaka, S. V. Khare, V. Petrova, D. D. Johnson, I. Petrov, and J. E. Greene, Phys. Rev. B **67**, 035409 (2003).
- ¹⁴S. Dieluweit and M. Giesen, J. Electroanal. Chem. **524-525**, 194 (2002).
- ¹⁵E. Pichardo-Pedrero and M. Giesen, Electrochim. Acta **52**, 5659 (2007).
- ¹⁶H. Ibach, M. Giesen, and W. Schmickler, J. Electroanal. Chem. 544, 13 (2003).
- ¹⁷H. Ibach and W. Schmickler, Phys. Rev. Lett. **91**, 016106 (2003).
- ¹⁸T. Michely and J. Krug, Islands Mounds and Atoms: Patterns and Processes in Crystal Growth Far from Equilibrium, Springer

- Series in Surface Science Vol. 42 (Springer, Heidelberg, 2004).
- ¹⁹M. Ondrejcek, W. Swiech, M. Rajappan, and C. P. Flynn, Phys. Rev. B **72**, 085422 (2005).
- ²⁰ K. Besocke, Surf. Sci. **181**, 145 (1987).
- ²¹ J. Frohn, J. F. Wolf, K. Besocke, and M. Teske, Rev. Sci. Instrum. 60, 1200 (1989).
- ²²T. Michely and G. Comsa, Surf. Sci. **256**, 217 (1991).
- ²³M. Giesen, Prog. Surf. Sci. **68**, 1 (2001).
- ²⁴J. Ikonomov, Jül-Berichte Jül-4144, 2004.
- ²⁵ J. F. Wolf, B. Vicenzi, and H. Ibach, Surf. Sci. **249**, 233 (1991).
- ²⁶M. Poensgen, J. F. Wolf, J. Frohn, M. Giesen, and H. Ibach, Surf. Sci. **274**, 430 (1992).
- ²⁷M. Giesen, C. Steimer, and H. Ibach, Surf. Sci. **471**, 80 (2001).
- ²⁸G. Wulff, Z. Kristallogr. Mineral. **34**, 449 (1901).
- ²⁹S. Dieluweit, H. Ibach, M. Giesen, and T. L. Einstein, Phys. Rev. B 67, 121410(R) (2003).
- ³⁰H.-C. Jeong and E. D. Williams, Surf. Sci. Rep. **34**, 171 (1999).
- ³¹ P. J. Feibelman, J. S. Nelson, and G. L. Kellogg, Phys. Rev. B 49, 10548 (1994).
- ³²P. J. Feibelman, Phys. Rev. Lett. **81**, 168 (1998).
- ³³P. J. Feibelman, Phys. Rev. B **60**, 4972 (1999).
- ³⁴P. J. Feibelman, Surf. Sci. **463**, L661 (2000).
- ³⁵G. Boisvert, L. J. Lewis, and M. Scheffler, Phys. Rev. B **57**, 1881 (1998).
- ³⁶R. C. Nelson, T. L. Einstein, S. V. Khare, and P. J. Rous, Surf. Sci. 295, 462 (1993).
- ³⁷S. Durukanoglu and T. S. Rahman, Phys. Rev. B **67**, 205406 (2003).
- ³⁸A. R. Sandy, S. G. J. Mochrie, D. M. Zehner, G. Grübel, K. G. Huang, and D. Gibbs, Phys. Rev. Lett. 68, 2192 (1992).
- ³⁹ M. Bott, M. Hohage, T. Michely, and G. Comsa, Phys. Rev. Lett. 70, 1489 (1993).
- ⁴⁰M. Hohage, T. Michely, and G. Comsa, Surf. Sci. **337**, 249 (1995).
- ⁴¹M. Giesen, G. S. Icking-Konert, D. Stapel, and H. Ibach, Surf. Sci. **366**, 229 (1996).
- ⁴² A. Kara and T. S. Rahman, J. Phys.: Condens. Matter **18**, 8883 (2006).